Magnetic Resonance in Medicine 67:1644–1655 (2012)

Motion Correction for Myocardial T1 Mapping Using Image Registration with Synthetic Image Estimation

Hui Xue,[1]* Saurabh Shah,[2] Andreas Greiser,[3] Christoph Guetter,[1] Arne Littmann,[3] Marie-Pierre Jolly,[1] Andrew E Arai,[4] Sven Zuehlsdorff,[2] Jens Guehring,[3] and Peter Kellman[4]

Quantification of myocardial T1 relaxation has potential value in the diagnosis of both ischemic and nonischemic cardiomyopathies. Image acquisition using the modified Look-Locker inversion recovery technique is clinically feasible for T1 mapping. However, respiratory motion limits its applicability and degrades the accuracy of T1 estimation. The robust registration of acquired inversion recovery images is particularly challenging due to the large changes in image contrast, especially for those images acquired near the signal null point of the inversion recovery and other inversion times for which there is little tissue contrast. In this article, we propose a novel motion correction algorithm. This approach is based on estimating synthetic images presenting contrast changes similar to the acquired images. The estimation of synthetic images is formulated as a variational energy minimization problem. Validation on a consecutive patient data cohort shows that this strategy can perform robust nonrigid registration to align inversion recovery images experiencing significant motion and lead to suppression of motion induced artifacts in the T1 map. Magn Reson Med 67:1644–1655, 2012. © 2011 Wiley Periodicals, Inc.

Key words: cardiac MRI; T1 mapping; image registration; motion correction; MOLLI

Quantification of T1 relaxation is of great importance for the characterization of myocardial tissue to assess both ischemic and nonischemic cardiomyopathies (1). Before the administration of contrast, an elevated value of myocardial T1 is associated with edema which may be related to the inflammatory response to myocardial injury. Following the administration of a T1-shortening contrast agent, a shortened T1 corresponding to increased contrast agent concentration is associated with fibrotic scar or diffuse fibrosis which has a greater extracellular volume than normal (2). Quantification of this extracellular volume fraction based on measurement of pre- and postcontrast T1-maps is a topic of high current interest as a means of detecting diffuse fibrosis which is difficult to detect based solely on late enhancement imaging (3–8).

[1]Siemens Corporate Research, Princeton, New Jersey, USA.
[2]CMR R&D, Siemens Medical Solutions USA, Inc., Chicago, Illinois, USA.
[3]Imaging & IT Division, Siemens AG, Healthcare Sector, Erlangen, Germany.
[4]Laboratory of Cardiac Energetics, National Institutes of Health, National Heart, Lung and Blood Institute, Bethesda, Maryland, USA.
*Correspondence to: Hui Xue, Ph.D., Siemens Corporation, Corporate Research, 755 College Road East, Princeton, NJ 08540.
E-mail: hui-xue@siemens.com

Received 10 June 2011; revised 17 July 2011; accepted 25 July 2011.
DOI 10.1002/mrm.23153
Published online 29 August 2011 in Wiley Online Library (wileyonlinelibrary.com).

While in vivo T1 quantification has been widely utilized in neuro and musculoskeletal imaging (9), T1 mapping of the heart remains a challenge mainly due to cardiac and respiratory motion (10). The normal T1 value of myocardium is approximately 950 ms at the field strength of 1.5T, which is on the order of the cardiac cycle (11). A modified Look-Locker inversion recovery (MOLLI) sequence was recently developed for myocardial T1 mapping (12). This pulse sequence is ECG triggered and acquires data at end-diastole when the heart is reasonably stationary. Unlike the standard Look-Locker T1 mapping which samples the recovery curve in constant intervals after an initial preparation pulse, this MOLLI sequence, as shown in Fig. 1, splits the sampling of recovery curve across multiple heart-beats. To obtain sufficient samples for accurate T1 estimation at the desired inversion times (TIs), multiple inversions are used with a number of images acquired for each inversion. All images are acquired at the same end-diastolic phase. Typically 6 to 11 inversion recovery (IR) images are acquired at different TI times as constrained by the limit of reasonable breath-hold duration (2,8,12,13).

A typical MOLLI scan performs two or three successive Look-Locker experiments and acquires images at the same cardiac phase. While this scheme may largely suppress the influence of cardiac motion, the myocardium does not always remain still across all images mainly due to undesired patient breathing. This is more problematic for subjects who are unable to hold their breath or uncooperative. Respiratory motion due to a failure of breath-holding or due to diaphragmatic drift could, if uncorrected, lead to errors in the pixel-wise estimation of T1 and degrade final maps. Respiratory motion correction is thus necessary for accurate T1-mapping. Figure 2 illustrates motion of the heart and corresponding mismatch while propagating myocardial contours during a breath-held acquisition.

Single shot cardiac imaging techniques which rely on retrospective motion correction for signal enhancement using multiple measurements typically use simple pairwise image registration methods (14–19). Successful applications include myocardium perfusion imaging (14), T2 mapping (15), free-breathing real-time cine (16), fat-water separation imaging (17), and delayed enhancement imaging (18,19). Unlike all these scenarios where image registration was directly applied to aligning multiple single-shot frames, the unique challenge to registration of inversion recovery images acquired at different TIs is due to the large variations in image contrast. Image registration is particularly difficult for images acquired close to the signal null-point. Different tissue species

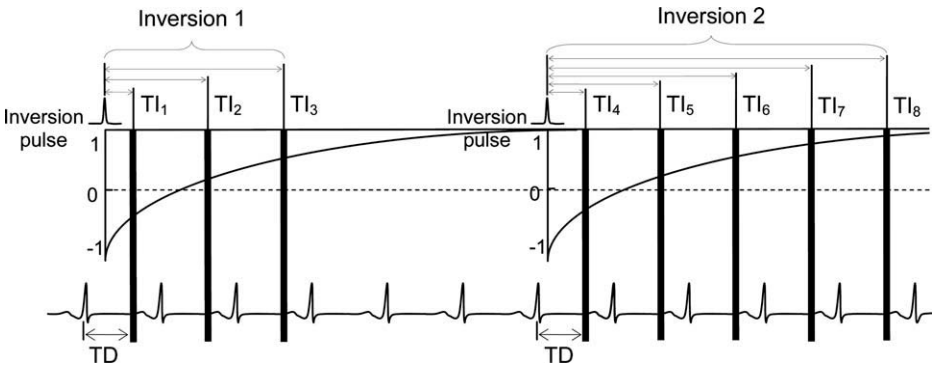

FIG. 1. A MOLLI sequence scheme shows two sets of inversions (Look-Locker experiments) were performed with increasing inversion time (TI) within one breath-hold. A total of eight images are acquired (three from first inversion and five from the second), as shown by the vertical bars. Images were acquired with the specific trigger delay (TD) to select the end-diastole. Each R-R interval is measured and the actual values of inversion time (TI) are used for T1-mapping.

with differing values of T1 such as blood, fat, normal myocardium, edematous myocardium, and infarcted myocardium will experience signal nulling at different TIs. Partial volume cancellation at the boundaries between pixels of different T1s will occur when the two species are out-of-phase which further confounds the image registration problem. At certain values of TI there is little or no contrast between adjacent tissues such as blood and myocardium. The change in contrast and appearance may be so significant that registration using either intensity or information based metrics may experience problems as evidenced in Fig. 3. It is not practical to find a set of TI values that avoid these problems due to the number of different expected values of T1.

In this study, we propose a novel motion correction algorithm based on estimating motion-free synthetic images presenting similar contrast to original MOLLI data by solving a variational energy minimization problem using a partial differential equation. Robust motion correction can be achieved by registering synthetic images to corresponding MOLLI frames. By this way, the difficulty of handling large variations of image contrast of inversion recovery is bypassed. The proposed technique was implemented into the MR reconstruction software and its effectiveness was verified in vivo on a large cohort of patient datasets which were consecutively acquired. We will show here that direct registration of MOLLI with a fixed reference frame leads to poor performance in a large percentage of cases while the proposed technique is highly robust against contrast changes and capable of correcting MOLLI images with different motion patterns and contrast concentrations. With the accurate correction of myocardial motion, the improved T1 mapping can be achieved with suppressed smearing artifacts around myocardium.

MATERIALS AND METHODS

We propose to solve the challenge of changing image contrast by exploiting the known exponential form of inversion recovery and treating the motion and inversion recovery as a joint estimation problem. This is done with an iterative approach based on initial T1 estimates and the generation of a series of motion free synthetic inversion recovery images which are used at each TI for registration with the measured MOLLI images. The initial T1-map is estimated using images acquired at the shortest and longest values of TI, which results in a crude estimate of T1 sufficient to initialize the iterative process. It was determined that although the contrast between the short and long TI images is not identical, these images were suitable for registration since they avoided the

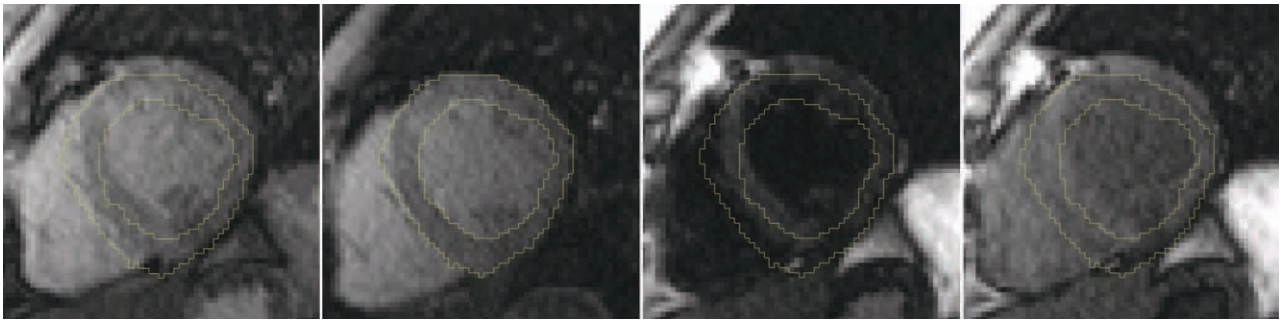

FIG. 2. A typical MOLLI acquisition with two inversions. Four of eight images are shown here. With the contour overlay (extracted from the second image), it is clear that myocardium motion between heart-beats can be severe. Image registration is particularly difficult for images acquired close to the signal null-point (e.g., the third image in this example), where the signal of blood and myocardium are completely inverted compared to other time points. [Color figure can be viewed in the online issue, which is available at wileyonlinelibrary.com.]

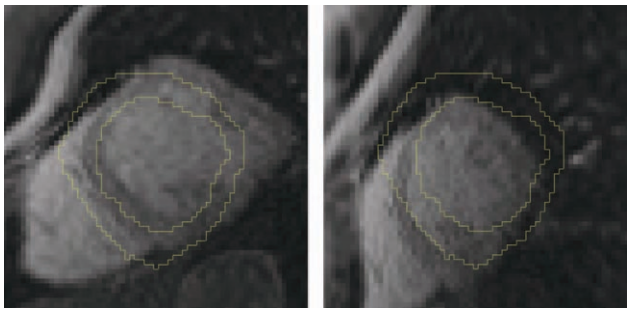

FIG. 3. Failed registration of aligning the second image in Fig. 2 to the third using cross-correlation (left) and mutual information (right). The inverted contrast between blood and myocardium and surround tissues make the direct registration a difficult task. [Color figure can be viewed in the online issue, which is available at wileyonlinelibrary.com.]

problem of tissue nulling and partial volume cancellation. The negative values occurring at short TIs are reconstructed as positive following conventional magnitude reconstruction. From the initial estimate of T1 at each pixel, synthetic images are calculated for each of the TI values corresponding to the measured data. The synthetic images are all at a fixed respiratory position and, importantly, each synthetic image has similar contrast to the corresponding measured image, making them suitable for intensity based image registration. Figure 4 illustrates the entire process for MOLLI T1 mapping with synthetic image estimation.

Energy Definition of Synthetic Image Estimation

With the initial rough estimation of T1 recovery, the synthetic image is computed by solving an energy minimization process. Given a group of N frames $I(x,y,t_n), n = 1,2,\ldots,N$ as inversion recovery images with different TIs t_n, the synthetic image $M(x,y,t_n), n = 1,2,\ldots,N$ is defined as a function to minimize the following energy functional:

$$M(x,y,t) = \underset{M}{argmin}\, E(M,I,S,w)$$

where the functional $E(M, I, S, w)$ is defined as:

$$E(M,I,S,w) = \iiint_{\Omega} \begin{bmatrix} (I(x,y,t) - M(x,y,t))^2 \\ +\alpha \cdot w(x,y) \cdot \left(M_x^2 + M_y^2\right) \\ +\beta \cdot (|S(x,y,t)| - M(x,y,t))^2 \end{bmatrix} dxdydt \quad [1]$$

Here $I(x,y,t_n)$ are the acquired MOLLI data, $S(x,y,t_n)$ are the inversion recovery images calculated from the initial T1 parameter fitting, M_x and M_y are 1st order partial derivatives of synthetic images, and the weighting w is described later. The integral is calculated over the entire image sequence. For the inversion recovery MOLLI sequence, the signal intensity of a pixel (x,y,t_n) is defined by the following three-parameter model (20):

$$\begin{aligned} S(x,y,t_n) &= A(x,y) - B(x,y) \times \exp(-t_n/T1^*(x,y)) \\ T1(x,y) &= T1^*(x,y) \times (B(x,y)/A(x,y) - 1) \end{aligned} \quad [2]$$

where A, B, and T1* are estimated by a three parameter fit to the measured data after the "polarity" has been restores as described next. In Eq. 2, t is the accumulative time from the inversion pulse. T1* is the apparent, modified T1 in a Look-Locker experiment. The inversion recovery described by Eq. 2 results in images that are negative at short TI and become positive after T1-recovery. However, the measured images are positive after magnitude reconstruction, losing the true signal polarity. The approach followed here restores the polarity as presented in (21) by a multifitting approach. The initial fit assumes that alls data points are positive; the second fit inverts the first data point, the third inverts the first two points, and so on. Finally, the case with the lowest residual error is selected.

The rationale of Eq. 1 is explained as follows. The first term constrains the distance between synthetic images and original MOLLI images. The second term is the regularizer. It is added to penalize the occasional errors in the original T1 estimate and keep the sufficient SNR of synthetic image. This term does not constrain the smoothness of the temporal behavior. The last term is added to minimize the distance between estimated images and MOLLI signal recovery curve. As the MOLLI signal recovery curve (Eq. 2) is smooth, this term actually implicitly constrains the temporal smoothness of estimated synthetic images.

The weight function $w(x, y)$ is added to keep the edge sharpness in the estimated synthetic image. This function is based on the observation that pixels of same tissue type tend to have the similar signal curve. Therefore, $w(x, y)$ is defined as the sum of correlation coefficients between a pixel and its four neighbors. If the weight for a pixel is smaller than an empirically selected threshold (0.75 for all experiments), it is set to be zero to completely penalize the any smoothing for this pixel.

Minimization Algorithm

Following the calculus of variation (22), the Eq. 1 can be minimized by solving the following Euler equation:

$$\alpha \cdot w(x,y) \cdot \left(\frac{\partial^2 M}{\partial x^2} + \frac{\partial^2 M}{\partial y^2}\right) - (1+\beta) \cdot M(x,y,t) + I(x,y,t) + \beta \cdot S(x,y,t) = 0 \quad [3]$$

Here the second-order partial derivatives are the natural derivation of regularization item.

Equation 3 can be solved by treating $M(x, y, t)$ as functions of evolution parameter k and solving:

$$\frac{\partial M}{\partial k} = \alpha \cdot w(x,y) \cdot \left(\frac{\partial^2 M_k}{\partial x^2} + \frac{\partial^2 M_k}{\partial y^2}\right) - (1+\beta) \cdot M_k(x,y,t) + I(x,y,t) + \beta \cdot S(x,y,t) \quad [4]$$

To set up the iterative solution, let the evolving step size be Δk. The $\partial M/\partial k$ is computed using the forward difference. The iterative solution of synthetic images is given as follows:

$$M_{k+\Delta k} = M_k + \Delta k \cdot \begin{bmatrix} \alpha \cdot w(x,y) \cdot \left(\frac{\partial^2 M_k}{\partial x^2} + \frac{\partial^2 M_k}{\partial y^2}\right) - (1+\beta) \cdot M_k(x,y,t) \\ +I(x,y,t) + \beta \cdot S(x,y,t) \end{bmatrix} \quad [5]$$

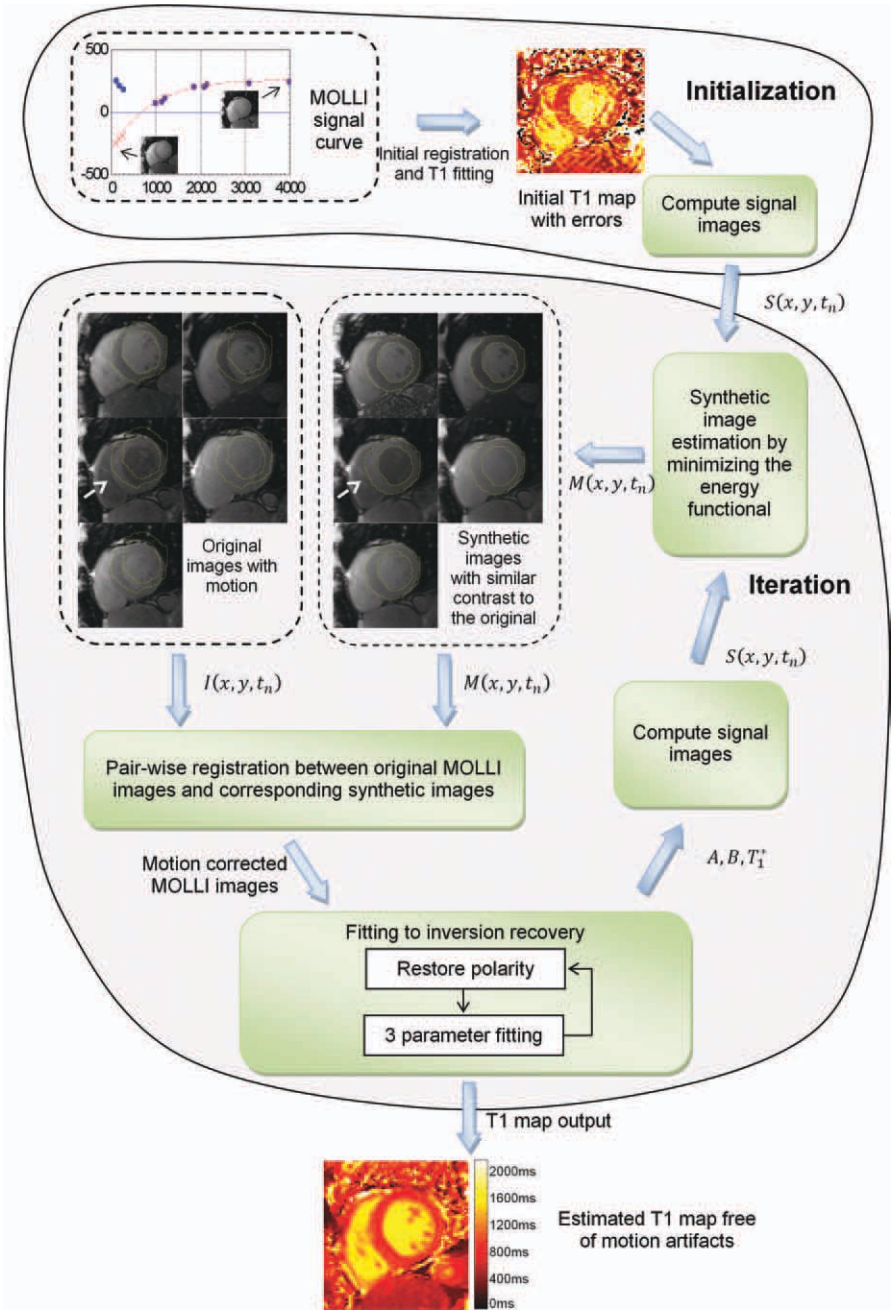

FIG. 4. Schematic diagram of motion correction for T1 MOLLI series based on an iterative approach using synthetic image estimation. The estimated motion-free synthetic images show similar contrast to the corresponding original images enabling intensity based pair-wise image registration.

The steady-state solution of Eqs. 4 and 5 is the desired solution of Euler equation. The resulting model images will minimize the energy function defined in Eq. 1. Note that Eq. 4 is a generalized diffusion equation. The convergence of this kind of equation is theoretically guaranteed if the iteration step Δk is sufficiently small and second-order derivatives are bounded (23). In all experiments, the convergence was considered to be reached if the reduction of energy function was less then 1e-3 which was generally fulfilled in less than 25 iterations.

To stably solve the Eq. 4, the second-order derivatives are estimated under the scale-space concepts by convolving the synthetic image M_k(x, y, t) with the second-order derivative of a small gaussian kernel (24):

$$\frac{\partial^{m+n} M(x,y,t_n)}{\partial x^m \partial y^n} = \frac{\partial^{m+n} g_\sigma(x,y)}{\partial x^m \partial y^n} * M(x,y,t_n) \qquad [6]$$

g_σ(x, y) is the gaussian kernel with the standard deviation σ. m, n ε {0,1,2} and $m + n \leq 2$.

Besides the iterative variational solution of the energy minimization problem, the partial differential equation define in Eq. 3 can be discretized and lead to a direct solution as well. Reformat the N frames $I(x, y, t_n)$,n = 1,2,. . .,N as a 1D vector:

FIG. 5. Plot of T1 fitting residual errors for the MOLLI series in Fig. 4. From left to right: residual errors of original images, errors of motion corrected images after the first, second and third iteration. For this dataset, the most significant improvement was achieved after the first iteration. More iterations lead to stable residual errors.

$$\tilde{\mathbf{I}} = [I(1,1,1), I(2,1,1), \cdots, I(N_x,1,1,\cdots, I(N_x,N_y,1), \cdots, I(N_x,N_y,N)] \quad [7]$$

N_x is the image size along the x dimension and N_y is the image size along the y dimension. N is the number of images acquired. Similarly, the synthetic and signal images can be converted as $\tilde{\mathbf{M}}$ and $\tilde{\mathbf{S}}$. In this formulation, the energy function is :

$$\tilde{E}(\tilde{\mathbf{I}},\tilde{\mathbf{M}},\tilde{\mathbf{S}},\mathbf{w}) = (\tilde{\mathbf{I}}-\tilde{\mathbf{M}}) \cdot (\tilde{\mathbf{I}}-\tilde{\mathbf{M}})' + \alpha \cdot \sum_{d=1}^{4} (\tilde{\mathbf{M}}\cdot\mathbf{D}_d)\cdot\mathbf{w}_d \cdot (\tilde{\mathbf{M}}\cdot\mathbf{D}_d)' + \beta\cdot(\tilde{\mathbf{S}}-\tilde{\mathbf{M}})\cdot(\tilde{\mathbf{S}}-\tilde{\mathbf{M}})' \quad [8]$$

Here the regularization item is calculated for the four-neighborhood of every pixel. D_1 to D_4 are the first order derivative operators formatting as a $N_xN_yN \times N_xN_yN$ matrix for four neighboring pixels. If the small derivative kernel is used such as basic forward or backward difference, D_d is highly sparse. Minimizing Eq. 8 leads to a system of linear equation by computing the derivative to $\tilde{\mathbf{M}}$:

$$\tilde{\mathbf{M}}\cdot\left[(1+\beta)\cdot\mathbf{Ind} + \alpha\cdot\sum_{d=1}^{4}\mathbf{D}_d\cdot\mathbf{w}_d\cdot\mathbf{D}_d'\right] = \tilde{\mathbf{I}} + \beta\cdot\tilde{\mathbf{S}} \quad [9]$$

Ind is the identity matrix.

The synthetic image can be computed by solving either Eq. 5 or 9. In practice, we observed that both methods lead to similar results, while the former is more efficient as most computation can be done on a per-pixel basis. The matrix inversion in Eq. 9, although appearing as a direct solution, generally requires an iterative solver such as conjugate gradient due to the size of image matrix involved. Thus, the solver derived from the Euler equation was used in following experiments.

Once the synthetic image is estimated, the registration is performed between every synthetic and corresponding MOLLI images. In practice, we iterated this process twice to further correction all residual motions. For the first iteration, the first and last time points were selected for initial T1 fitting. On the second run, the first and last two points were used. The residual T1-fitting error is displayed in Fig. 5 to illustrate the process.

Image Registration

Given the synthetic frames estimated from the energy minimization process, robust motion correction can be achieved by registering the synthetic images to the corresponding measured MOLLI images in a frame-by-frame manner, since the contrasts of these images are very close. Because of the nonrigid nature of cardiac deformation, a fast variational nonrigid image registration framework (25) is applied as the working-engine. This approach can be considered as an extension of the classic optical flow method. In this framework, a dense deformation field is estimated as the solution to a calculus of variation problem, which is solved by performing a compositional update step corresponding to a partial differential transport equation. The regularization is added by low-pass filtering the gradient images which are in turn used as velocity field to drive the transport equation. To speed up the convergence and avoid local minima, a multiscale image pyramid is created. We selected the local cross correlation as the image similarity measure, as its explicit derivative can be more efficiently calculated than mutual information and still general enough to cope with noise and intensity difference between synthetic and real images, as the former will present similar contrast compared to the later, but no guaranty can be made that rigorous pixel-wise intensity consistency can be produced.

Inline T1 Mapping

With the myocardial motion corrected, the T1 map is generated via the pixel-wise curve fitting using the three parameter signal model (Eq. 2). The downhill simplex minimization algorithm proposed by Nelder and Mead (so-called Nelder–Mead method (26)) is applied. We observed that the simplex method consistently produced similar outputs as the Levenberg-Marquardt minimization (27), while our experiments show that the former is more efficient probably since this method requires only function evaluations. The downhill simplex minimization was thus used for all processing. After the signal polarity correction, the maximal intensity was used to initialize A, approximating the fully recovered magnetization. B was initialized as A minus the minimal intensity, approximating the magnetization at $t_n = 0$. T1* was initialized as the linearly interpolated zero-crossing time

estimated from the polarity corrected signal intensity curve.

To make the proposed techniques accessible to clinicians, all processing steps were implemented within the Image Calculation Environment of Siemens MRI system. It provides the functionality of fully automated inline T1 mapping. The processing immediately starts after the reconstruction of all MOLLI images and sends original inversion recovery images, motion corrected images and derived T1 maps to the image database. For the experiments conducted in this study, the MR reconstruction computer was equipped with 8 CPU cores and 16 GB of RAM. Multithreading was utilized when performing the pixel-wise fitting for T1 value estimation. Typical processing time was less than 10 s for one slice, including synthetic image estimation, frame-to-frame registration and the final map computation.

In Vivo Study

MOLLI images were acquired for 50 consecutive patients (27 men, 23 women; mean age 55.4 ± 13.2 years) using a clinical 1.5T MR scanner (MAGNETOM Espree, Siemens AG Healthcare Sector, Erlangen, Germany) at the National Heart, Lung and Blood Institute, Bethesda, Maryland. This study was approved by the local Institutional Review Board, and all subjects gave written informed consent to participate. The MR sequence parameters included: inversion recovery prepared MOLLI with balanced SSFP readout, TR = 2.4/TE = 1.05 ms, acquired matrix 192 × 130, flip angle 35°, in-plane spatial resolution 1.875 × 2.077 mm^2, rectangular FOV 360 × 270 mm^2, slice thickness 6 mm, bandwidth 1042 Hz/pixel. Applied MOLLI protocol consisted of two IR prepared and ECG-gated acquisitions (8 images acquired within 11 heart-beats, 3 from the first IR, and 5 from the second with an interval of three heart-beats to ensure the fully recovery of longitudinal magnetization) which were performed within one breath-hold. For every patient, both pre- and postcontrast acquisitions were performed for either 1 or 2 slices, resulting in a total of 230 MOLLI series (140/90 pre/postcontrast, 128/102 short/long axis, 93/30/5 medial/basal/apical slices for short axis, 90/12 4-chamber/2-chamber view for long axis).

Quantification of Motion Correction

To quantify the accuracy of motion correction, two frames were selected by a human rater for every MOLLI series. Myocardium was manually delineated on each selected image. The criteria of selection are a) myocardium shows discernible movement and b) myocardium bears enough contrast. For series where motion is visible, frames exhibiting movement were picked to highlight the improvement of correction. For series where myocardium is still, frames showing best contrast were picked to minimize the errors of manual segmentation.

After motion correction, the segmented myocardium was propagated to the corrected images using the deformation fields outputted by the image registration. An ideal motion correction will lead to a perfect overlap between segmented myocardium from two frames. Therefore, the overlap rate before and after motion correction was computed as the Dice similarity coefficient (DSC) (28). For two segmented regions A and B, the DSC is defined as:

$$DSC = \frac{2 \times area(\mathbf{A} \cap \mathbf{B})}{area(\mathbf{A}) + area(\mathbf{B})}$$

This value will be 1 for a perfect overlap and 0 for nonoverlap.

To further evaluate the performance of motion correction, the false positive (FP) and false negative (FN) errors are also computed. FP is defined as the percentage area of segmented myocardium in the first frame that is not labeled in the second and FN is defined as the percentage area of myocardium in the second that is not labeled in the first.

Because the cardiac motion can be nonrigid in its nature, the myocardium boundary errors which is defined as the mean distance between endo/epi contours of two frames are computed for all series as well. While DSC will capture the bulk motion due to failed breath-holding, myocardium boundary error could highlight the local myocardial deformation probably due to imperfect cardiac gating.

To avoid possible bias introduced by only segmenting two frames per MOLLI series, a second human rater was asked to randomly pick up one-third of all 230 series, at least one series per patient. This results in a total of 56 series (32/24 pre/postcontrast, 46/10 short/long axis). Manual delineation of myocardium was performed on every frame for these 56 series by the second human rater. The segmented myocardium was propagated to the corresponding motion corrected images using the deformation fields. Misalignment measures (DSC, FP, FN, and myocardium boundary error) were computed for every frame.

The inter-rater variability was quantified by comparing the manual delineation of two human raters. For every frame segmented by both two raters (2 frames per series for those 56 series), all four measures were computed to estimate the variability.

To quantify the influences of motion correction on T1 values, for those cases where hearts remain completely still, the fluctuation of T1 values before and after correction ($T1_{ori}$ and $T1_{moco}$) is quantified by computing the mean of relative absolute difference (MAD) for all N pixels within the myocardium:

$$MAD = \frac{1}{N}\sum_{i=1}^{N} |(T1^i_{ori} - T1^i_{moco})/T1^i_{ori}|$$

RESULTS

To verify the necessity of motion correction for inversion recovery images acquired across multiple heart-beats, visual reading was performed for all datasets which were classified into two categories according to the presence of myocardium motion. Noticeable motion was not found in 138 series (no motion, 60%) and was found in 92 series (with motion, 40%). This emphasizes the necessity

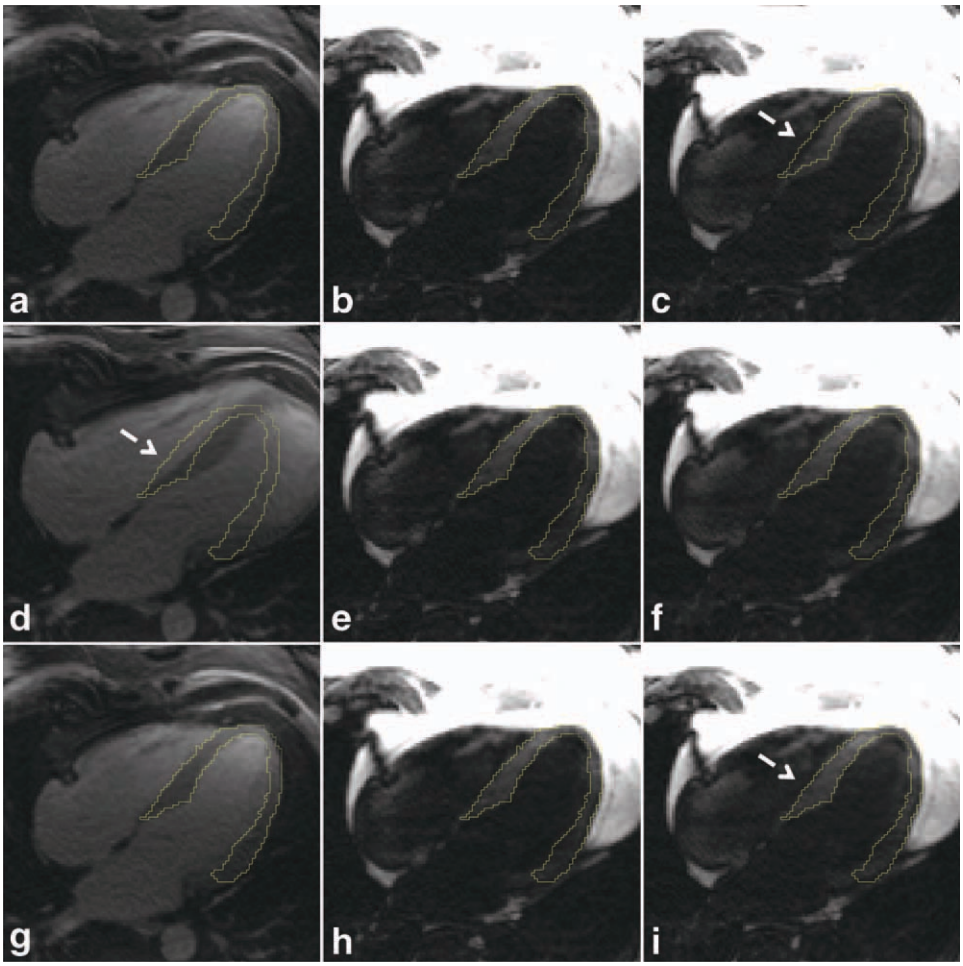

FIG. 6. Example of MOLLI motion correction. Three of eight MOLLI images are shown. **a–c:** Original images showing significant motion. **d–f:** Results by directly applying nonrigid registration causing incorrect deformation. **g–i:** Motion correction based on synthetic image estimation. [Color figure can be viewed in the online issue, which is available at wileyonlinelibrary.com.]

of the motion correction. Typical examples are given in Figs. 6–8.

To reveal the inadequate robustness of directly registering MOLLI images using a fixed reference (this strategy is referred as 'direct registration' hereafter), the same fast variational nonrigid image registration algorithm was used (same as used for registration with synthetic model images). In current experiments, all frames within a series were registered to the 5th frame which typically exhibited the best contrast between the myocardium and blood. Although the first or last frames have higher SNR, there is insufficient contrast due to fully inversed or recovered magnetization. Due to the variation of T1 values among different tissues and subjects, it is difficult to select a frame consistently presenting good contrast between myocardium and blood-pool.

The direct registration with a fixed reference among MOLLI images with largely varying contrast often leads to unrealistic deformation or failed registration. To measure the failure rate, visual reading was performed on all outputs of the direct registration strategy and unrealistic deformation was found in 176 cases among the whole cohort (77%). In many cases, even the original myocardium was still, the significant contrast changes, especially around the epi-cardial fat region, can drive the registration in the wrong way. This phenomenon was illustrated in Figs. 6–8. Given the large percentage of failure rate of direction registration, no attempt was made to further quantify the performance of direct registration with fixed reference, because a motion corrected series unlikely offer adequate diagnostic confidence if one or more frames show severe unrealistic deformation.

For all series where motion is discernible, the proposed method corrects the myocardial movement successfully (Figs. 6–8). Figure 9a shows a bar chart summarizing quantitative measures for cases with myocardial movement. After motion correction, the overlap ratio DSC is increased significantly ($P < 0.05$) and both FP and FN are reduced ($P < 0.05$). The myocardium boundary errors go down from 1.4 mm to 1.2 mm, showing the local myocardial deformation is corrected by the synthetic image estimation based registration ($P < 0.001$). The paired *t*-test was used to compare all four measures.

Unlike the direct registration, proposed method is robust against contrast changes. For all cases where myocardium is still, the motion correction does not introduce unwanted deformation, which is supported by the close DSC ratios before and after motion correction, as presented in Fig. 9b.

For all cases where heart remains still, the mean MAD is 0.010 ± 0.018, indicating an averaged T1 fluctuation of less than $\sim$3% after motion correction, which could be due the intensity interpolation during the image registration. Furthermore, visual comparison of T1 maps

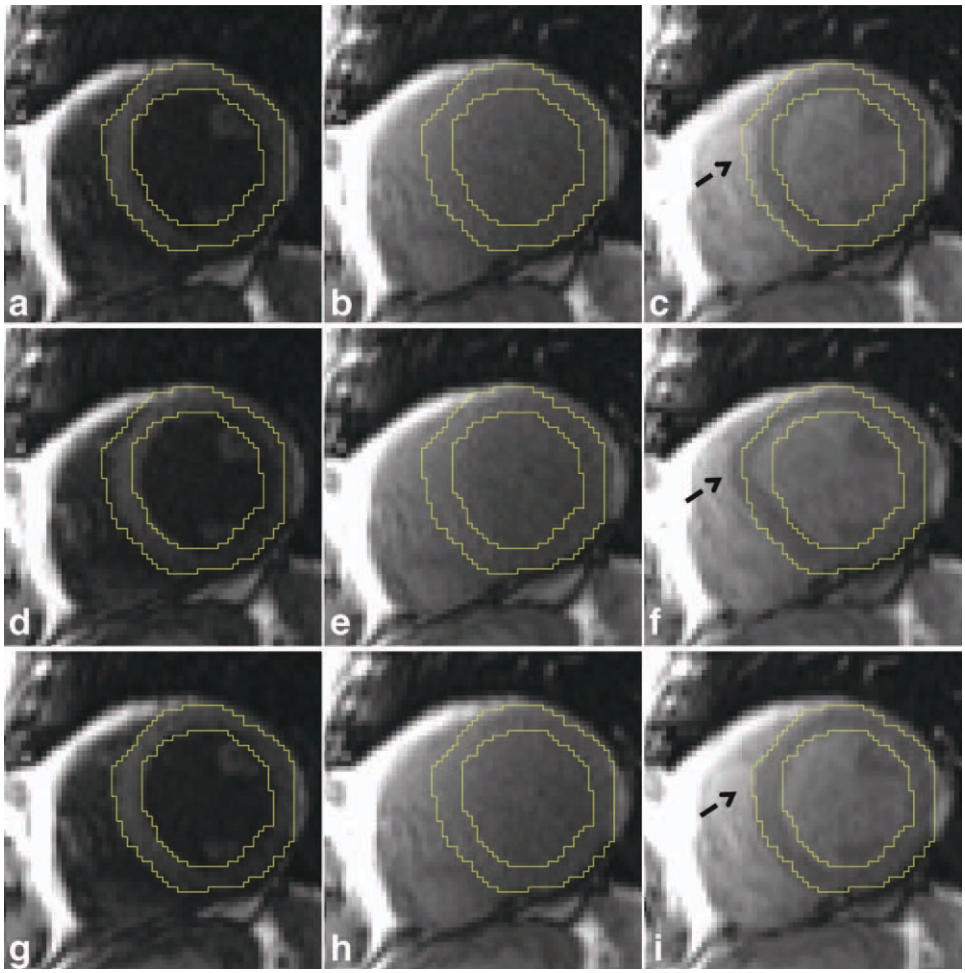

FIG. 7. Example of MOLLI motion correction. **a–c:** Original images showing noticeable motion. **d–f:** Results by directly applying nonrigid registration causing incorrect deformation. **g–i:** Motion correction based on synthetic image estimation. [Color figure can be viewed in the online issue, which is available at wileyonlinelibrary.com.]

before and after motion correction does not lead to the exposure of small focal regions where T1 values show discernible variations. The maps before and after correction are visually identical.

T1 mapping of heart is required for both pre and postcontrast scenario. This is essential to compute the extracellular volume fraction in either pixel-wise or segmental manner. The motion correction therefore should be fully functional for both pre and postcontrast to maximize its clinical applicability. With the observation that proposed method show consistent performance across the entire data cohort, for all moved cases, four motion correction statistics were computed separately for both pre and post series. Table 1 listed the results showing improved myocardial alignment was achieved for both scenarios. While the improvement of motion correction is significant for both pre and postcontrast cases, the performance does not show significant bias towards either scenarios ($P > 0.1$ for all four measures).

To avoid possible bias introduced by only segmenting two frames per series, a total of 56 series were randomly selected by the second human rater, including 34 "no motion" and 22 "with motion" series. The human rater delineated myocardium from every frame. For the 'no motion' cases, the mean overlap ratio DSC is 0.850 ± 0.068. After motion correction, the DSC is 0.862 ± 0.051. The FP, FN, and BSE show small fluctuations (before motion correction: FP 0.137 ± 0.071; FN 0.152 ± 0.088; BSE 1.176 ± 0.430 mm; after motion correction, FP 0.150 ± 0.082; FN 0.148 ± 0.080; BSE 1.165 ± 0.534 mm). No statistically significant differences were found for 'no motion' cases ($P > 0.1$ for all four measures). For the moved cases, DSC was increased significantly from 0.779 ± 0.136 to 0.828 ± 0.085 after motion correction ($P < 0.001$). FP, FN and BSE were decreased significantly (FP: 0.222 ± 0.160 to 0.172 ± 0.117, $P < 0.001$; FN: 0.196 ± 0.117 to 0.172 ± 0.087, $P < 0.001$; BSE: 1.789 ± 1.009 mm to 1.337 ± 0.501 mm, $P < 0.001$).

The inter-rater variability was estimated by comparing the manual delineations of two human raters. The mean DSC for inter-rater variability is 0.853 ± 0.050. FP and FN are 0.129 ± 0.099 and 0.065 ± 0.037. The boundary error BSE (1.139 ± 0.369 mm) is less than one pixel (acquired pixel size: 1.875×2.077 mm^2). This validation, although not performed for every frame in current experiment, indicates that for the anatomy with simple geometry such as myocardium, the inter-rater variability is not severe and reasonable reproducibility can be achieved. In particular, DSC measures above 0.7 can be regarded as a satisfactory level of agreement between two independent segmentations (29). On the other hand, for frames where the contrast between myocardium and blood-pool is insufficient, the inter-rater variability might rise. But these frames are expected to have less

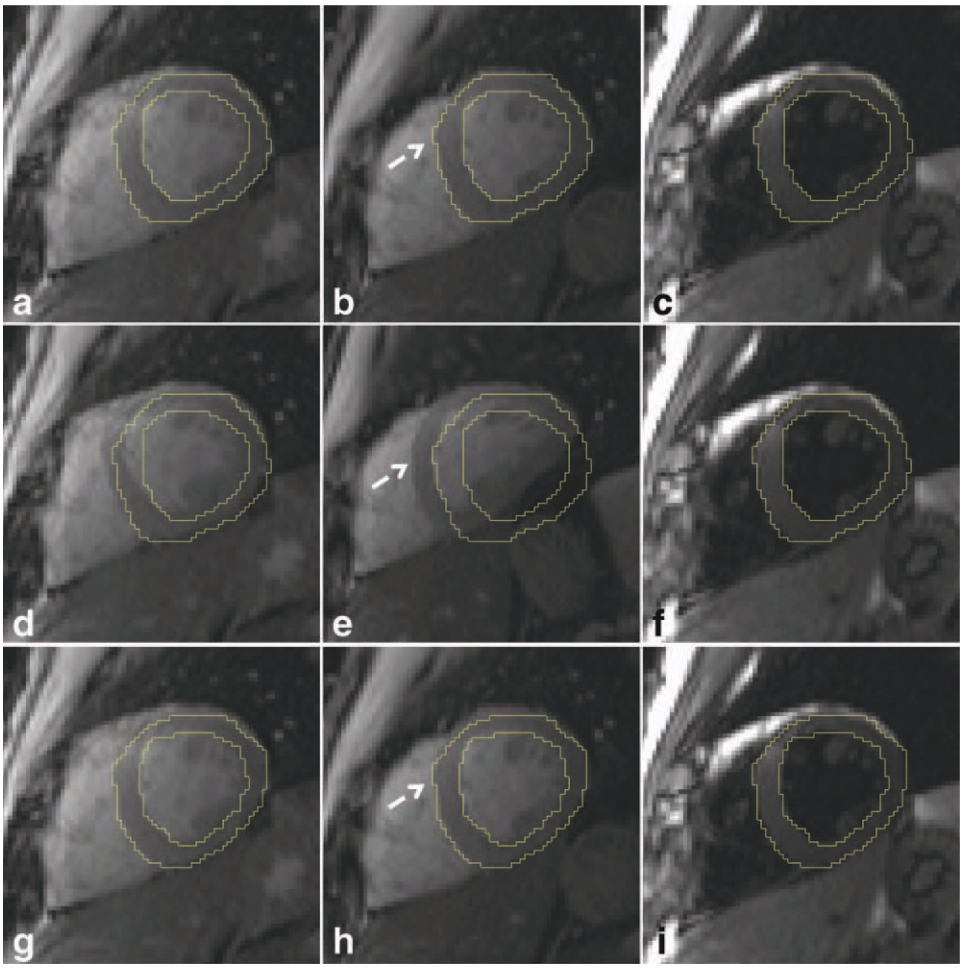

FIG. 8. Example of MOLLI motion correction. **a–c:** Original MOLLI images where myocardium is still in this case. **d–f:** Results by directly applying the nonrigid registration shows the failure of registration, as shown in (d–e). **g–i:** Motion correction based on synthetic image estimation. [Color figure can be viewed in the online issue, which is available at wileyonlinelibrary.com.]

influences on the final T1 values as small misalignments tends to be more benign.

T1 maps estimated from corrected inversion recovery images often show reduced motion artifacts. As an illustration, for patients who failed to hold the breath well, the T1 map after correction depicts the myocardium correctly while the maps from original images show smearing due to the heart motion (Fig. 10).

DISCUSSION

A method of motion correction for inversion recovery myocardial T1 mapping was developed and validated on a consecutive patient data cohort. With the insights to recognize that largely varying contrast causes major difficulty for robust alignment of MOLLI images, a solution was proposed to estimate intermediate synthetic images bearing similar contrast to the MOLLI images and performing motion correction based on those. We have shown that this scheme leads to highly robust motion correction and does not introduce unrealistic deformation.

Although the theory and derivation of synthetic image estimation was inspired by T1 MOLLI imaging, the problem formulation and its solutions are not limited to inversion recovery only. The formulation will hold if the signal model has an analytic expression or it can be estimated from the image data. For example, in the application of myocardial first-pass perfusion imaging, the independent component analysis has been utilized to extract a signal model and motion correction was achieved by registering the signal model, rather than original perfusion images (30). Other transformations to derive signal model could include Karhunen-Loeve transform and linear regression (31,32).

The entire process consists of pixel-wise T1 fitting, nonrigid image registration and synthetic image estimation. The computation time of frame-to-model registration was ~0.1 s per frame and for synthetic image estimation it was ~1 s. Within the current implementation, the most time-consuming step was pixel-wise curve fitting (~70% of total processing time). The reason is that to detect the polarity of MOLLI signal for every pixel in the image, the curve fitting computation of inversion recovery three-parameter model has to be performed multiple times until the lowest residual errors are found. Fortunately, since the pixel-wise fitting is independent from each other, the multithreading is employed for speedup. Given the fact that modern MR reconstruction hardware is often equipped with multiple CPU cores, the computational time of curve fitting can be decreased linearly. Besides the parallel computing, other means to avoid the multiple fitting could include performing the T1 estimation on the magnitude signal $|A(x,y) - B(x,y) \times \exp(-t_n/T1^*(x,y))|$ without trying to recover the polarity. It is likely that the

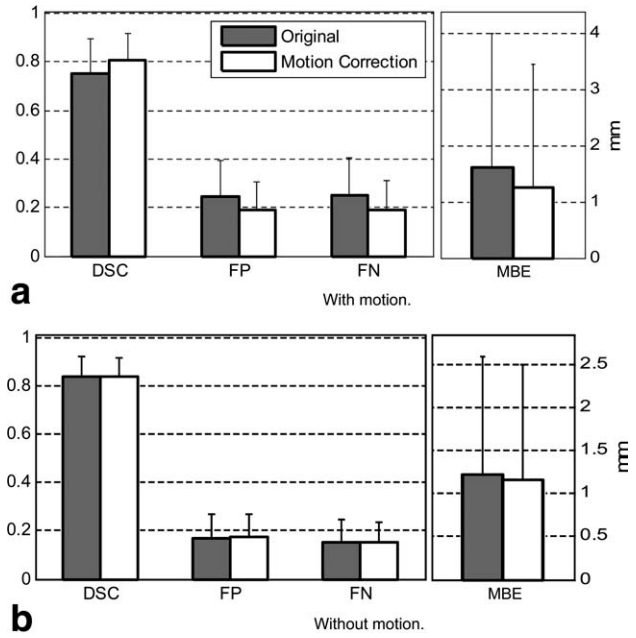

FIG. 9. Four measures to quantify the improvement of motion correction for better myocardial alignment. For cases with noticeable motion, the myocardium alignment is significantly better after correction. For cases without heart motion, the proposed method does not introduce undesired position changes of heart and local deformation.

discontinuity of signal derivative around the nulling point may degrade the fitting precision; however, the overall accuracy of T1 estimation could still be adequate for synthetic image estimation. Once the myocardial movement is suppressed, the multiple fitting can be applied only once to getting more accurate final T1 map. Other alternatives to accelerate pixel-wise curve fitting include the provision of better initialization for three parameter models by utilizing the local homogeneity of T1 values. The fitting outputs of one pixel can be used to initialize its neighbors if the correlation between their signal curves is sufficiently high. In this way, the number of iterations needed for optimization may be reduced, so does the total computational time. One drawback of this approach is that every pixel cannot be processed independently anymore and the efficiency of multithreading implementation may be compromised. This strategy has not been tested in current experiments as the current processing with multithreading is reasonable. On the platform where multicore hardware is not available, the local homogeneity of T1 values could certainly be helpful for further speedup.

One advantage of proposed method is its fully unsupervised nature. No preprocessing or user interaction is needed and motion corrected MOLLI images and T1 map are computed automatically. We found that it is a major advantage when boosting the clinical acceptance of proposed technique. As a result, all processing steps were implemented in the MR scanner as a part of reconstruction pipeline. The total computational time is less than 10 s for a slice. In the scenario that multiple slices are acquired to cover the myocardium, the processing for every slice could be performed in parallel. Other means to further gain speedup include performing background detection to mask out the air region. Clearly, no computation shall be done for those pixels.

The imaging protocol used in this study still requires performing the image acquisition within one breathhold. It is generally achievable in the clinical setting and reduces possible range of heart motion due to breathing. We have shown that even breath-holding is suggested ~40% acquired series in the data cohort present discernible motion, which indicates the necessity of effective motion correction. On the other hand, proposed method has some potential to correct in-plane motion of myocardium in a free-breathing acquisition. The image registration, even nonrigid approaches, may not be capable of correcting large through-plane motion if working on 2D frames (33). It can limit the applicability of proposed technique on datasets with large R-R interval changes, such as arrhythmias. One possible extension could be detecting and rejecting frames with strong through-plane motion from fitting and registration. To maintain the sufficient number of samples on the inversion recovery curve, more heart beats may be needed. It is a future research topic to extend current framework for free-breathing MOLLI T1 mapping and to handle varied R-R intervals.

A major challenge of MOLLI image registration is the loss of tissue contrast at certain TIs. That is, for some

Table 1
Quantitative measures of motion correction before and after contrast injection

	Pre contrast							
	Dice		FP		FN		MBE (mm)	
	ORI	MOCO	ORI	MOCO	ORI	MOCO	ORI	MOCO
Mean	0.726	0.795	0.271	0.209	0.276	0.201	1.791	1.343
STD	0.157	0.096	0.160	0.101	0.168	0.115	3.464	3.247
	Post contrast							
Mean	0.773	0.823	0.218	0.167	0.234	0.188	1.739	1.315
STD	0.133	0.124	0.142	0.136	0.139	0.124	1.752	1.576

ORI, original images; MOCO, motion correction.
Paired t-test, pre-contrast: Dice($P<0.05$), FP ($P<0.05$), FN ($P<0.05$), MBE ($P<0.01$) ; post-contrast: Dice ($P<0.05$), FP ($P<0.05$), FN ($P<0.05$), MBE ($P<0.01$).

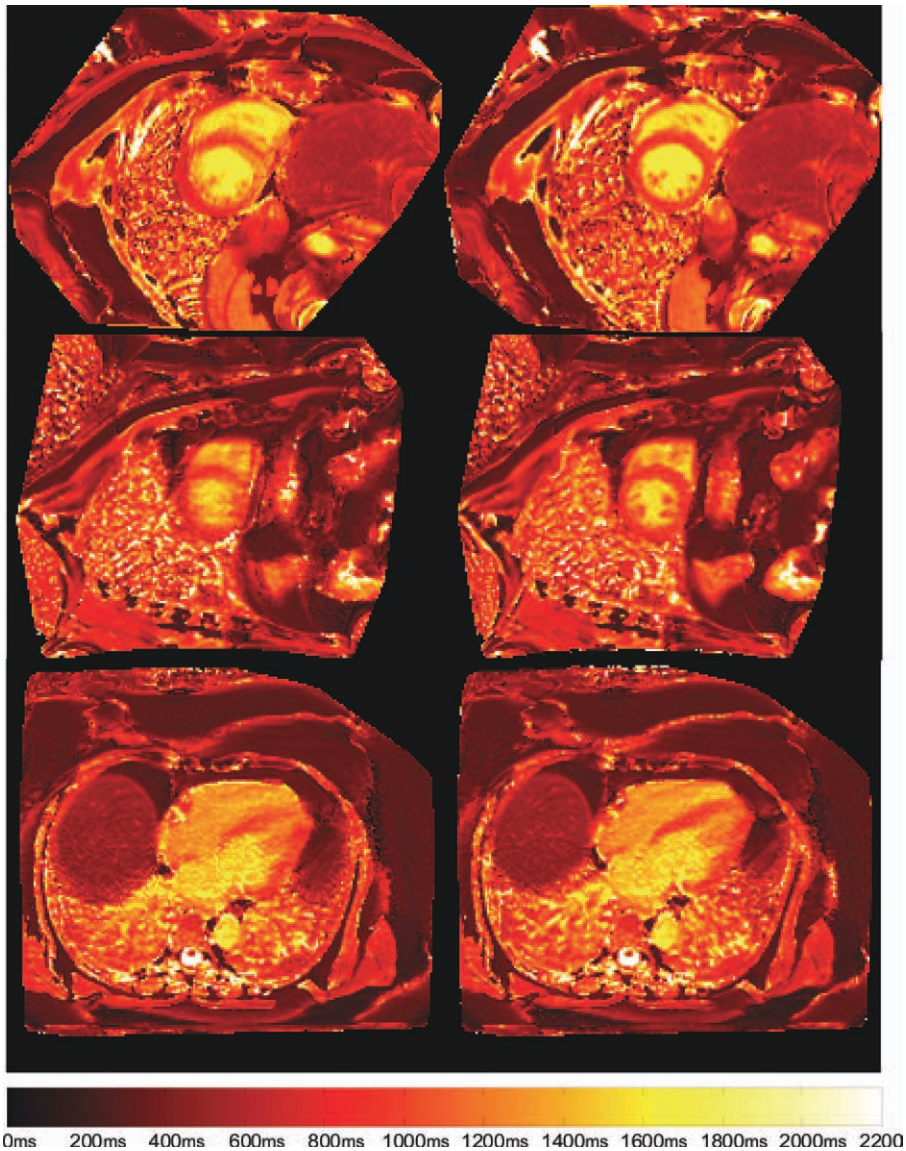

FIG. 10. Example of improved T1 mapping after motion correction. Left column: T1 maps of original MOLLI images indicating smearing on the myocardium due to imperfect breath-holding. Right column: Sharp myocardial boundary is recovered after motion correction using proposed technique. These images were from three different patients.

recovery time TIs, the myocardium is clearly visible while other unfavorable TIs could suppress the magnetization difference between blood-pool and myocardium. The registration between these frames is highly error-prone, as the contents presented in images are different. Even using image similarity measures such as mutual information or normalized mutual information, the robustness of registration was problematic. Mutual information metric may handle variation in contrast but do not cope well with image content occlusion.

It is found that the general idea of firstly estimating model images and subsequently registering individual images using the model has been previously employed in different applications (30). In this article, a motion correction method was developed for MR first-pass perfusion images. Here the model images were estimated using the perfusion signal model with curve fitting and myocardial motion was corrected by registering the perfusion images to corresponding model frames. Although there are similarities between this scheme and our approaches, MR perfusion images are saturation recovery (SR) prepared images that demonstrate fundamentally different contrast than the inversion recovery prepared images used for T1 mapping. In SR prepared images, the net magnetization is always intrinsically positive and the dynamic changes in signal intensity are relatively benign. In contrast, in inversion recovery images, the magnetization can be negative, positive or even zero depending on the time between the IR pulse and data acquisition, which introduces significant variations of tissue contrast between even adjacent frames. Such magnetization polarity information is lost in final MR images that only represent the magnitude of the magnetization. Therefore, previously described methods (14) that employ direct pair-wise alignment of perfusion images are not directly applicable to the T1 mapping. Another significant difference is the algorithms used to estimate model images. Specifically, in our scheme, model image estimation was formulated as an energy minimization problem and solved using a partial differential equation.

In contrast, curve fitting without further optimization was used for perfusion images. Although this simple strategy may work well for perfusion, it has limited applicability in the applications where there are significantly fewer samples of intensities and significantly higher variations in contrast among the samples.

CONCLUSIONS

We have presented a novel algorithm to perform the motion correction for myocardial T1 mapping using inversion recovery acquisition. The key idea is to estimate the synthetic images presenting similar contrast changes to original images by solving an energy minimization problem. This approach is fully automated and requires no preprocessing. Thus, it has been seamlessly integrated into the image acquisition and reconstruction pipeline and lead to inline generation of pixel-wise T1 map with motion correction. Our experiments illustrate the robustness and accuracy of this method, which will be the key for its clinical usage.

REFERENCES

1. Schulz-Menger J, Friedrich MG. Magnetic resonance imaging in patients with cardiomyopathies: when and why. Herz 2000;25: 384–391.
2. Ugander M, Bagi PS, Oki AJ, Chen B, Hsu L-Y, Aletras AH, Shah S, Greiser A, Kellman P, Arai AE. Quantitative T1-maps delineate myocardium at risk as accurately as T2-maps—experimental validation with microspheres. J Cardiovasc Magn Reson 2011;13 (Suppl 1):62.
3. Flett AS, Hayward MP, Ashworth MT, Hansen MS, Taylor AM, Elliott PM, McGregor C, Moon JC. Equilibrium contrast cardiovascular magnetic resonance for the measurement of diffuse myocardial fibrosis: preliminary validation in humans. Circulation 2010;122: 138–144.
4. Mewton N, Liu CY, Croisille P, Bluemke D, Lima JAC. Assessment of myocardial fibrosis with cardiovascular magnetic resonance. J Am College Cardiol 2011;57:891–903.
5. Schelbert EB, Testa SM, Meier CG, Ceyrolles WJ, Levenson JE, Blair AJ, Kellman P, Jones BL, Ludwig DR, Schwartzman D, Shroff SG, Wong TC. Myocardial extravascular extracellular volume fraction measurement by gadolinium cardiovascular magnetic resonance in humans: slow infusion versus bolus. J Cardiovasc Magn Reson 2011; 13:1–14.
6. Janardhanan R, Jiji RS, Brooks J, Epstein FH, Kramer CM, Salerno M. A comparison of methods for determining the partition coefficient of gadolinium in the myocardium using T1 mapping. J Cardiovasc Magn Reson 2011;13 (Suppl 1):77.
7. Ferreira VM, Piechnik SK, Dall'Armellina E, Karamitsos TD, Francis JM, Friedrich MG, Robson MD, Neubauer S. Quantification of acute myocardial injury by ShMOLLI T1-Mapping, T2-weighted and late gadolinium imaging in patients presenting with chest pain, positive troponins and non-obstructive coronary arteries. J Cardiovasc Magn Reson 2011;13 (Suppl 1):114.
8. Sibley CT, Huang J, Ugander M, Oki A, Han J, Nacif MS, Greiser A, Messroghli DR, Kellman P, Arai AE, Bluemke DA, Liu S. Myocardial and blood T1 quantification in normal volunteers at 3T. J Cardiovasc Magn Reson 2011;13 (Suppl 1):144.
9. Lin W, Song HK. Improved signal spoiling in fast radial gradient-echo imaging: applied to accurate T1 mapping and flip angle correction. Magn Reson Med 2009;62:1185–1194.
10. Messroghli DR, Plein S, Higgins DM, Walters K, Jones TR, Ridgway JP, Sivananthan MU. Human myocardium: single-Breath-hold MR T1 mapping with high spatial resolution—reproducibility study. Radiology 2006;238:1004–1012.
11. Flacke SJ, Fischer SE, Lorenz CH. Measurement of the gadopentetate dimeglumine partition coefficient in human myocardium in vivo: normal distribution and elevation in acute and chronic infarction. Radiology 2001;218:703–710.
12. Piechnik S, Ferreira V, Dall'Armellina E, Cochlin L, Greiser A, Neubauer S, Robson M. Shortened modified Look-Locker inversion recovery (ShMOLLI) for clinical myocardial T1-mapping at 1.5 and 3 T within a 9 heartbeat breathhold. J Cardiovasc Magn Reson 2010;12 (Suppl 1):69.
13. Messroghli DR, Radjenovic A, Kozerke S, Higgins DM, Sivananthan MU, Ridgway JP. Modified Look-Locker inversion recovery (MOLLI) for high-resolution T1 mapping of the heart. Magn Reson Med 2004; 52:141–146.
14. Xue H, Zuehlsdorff S, Kellman P, Arai A, Nielles-Vallespin S, Chefd-hotel C, Lorenz C, Guehring J. Unsupervised inline analysis of cardiac perfusion MRI. Lecture Notes Comput Sci 2009;5763:741–749.
15. Shivraman Giri YC, Shah S, Xue H, Guehring J, Zuehlsdorff S, Simonetti OP. T2 Mapping Using T2prepared-SSFP: Optimizing Echo Time, Flip Angle and Parameter Fitting. In: Proceeding of the Joint Annual Meeting ISMRM-ESMRMB, Stockholm, Sweden, 2010. p 2960.
16. Kellman P, Chefd'hotel C, Lorenz CH, Mancini C, Arai AE, McVeigh ER. High spatial and temporal resolution cardiac cine MRI from retrospective reconstruction of data acquired in real time using motion correction and resorting. Magn Reson Med 2009;62:1557–1564.
17. Kellman P, Hernando D, Shah S, Liang Z-P, Arai AE. Free-Breathing, Single Shot Fat-Water Separated Cardiac Imaging with Motion Corrected Averaging. In: Proceeding of the Joint Annual Meeting ISMRM-ESMRMB, Stockholm, Sweden, 2010. p 3662.
18. Kellman P, Larson AC, Hsu L-Y, Chung Y-C, Simonetti OP, McVeigh ER, Arai AE. Motion-corrected free-breathing delayed enhancement imaging of myocardial infarction. Magn Reson Med 2005;53:194–200.
19. Ledesma-Carbayo MJ, Kellman P, Arai AE, McVeigh ER. Motion corrected free-breathing delayed-enhancement imaging of myocardial infarction using nonrigid registration. J Magn Reson Imaging 2007;26: 184–190.
20. Sass M, Ziessow D. Error analysis for optimized inversion recovery spin-lattice relaxation measurements. J Magn Reson 1977;25: 263–276.
21. Nekolla S, Gneiting T, Syha J, Deichmann R, Haase A. T1 Maps by K-space reduced snapshot-FLASH MRI. J Comput Assist Tomogr 1992;16:327–332.
22. Gelfand IM, Fomin SV. Calculus of variations. Mineola, NY: Dover Publications; 2000.
23. Ames WF. Numerical methods for partial differential equations. New York, NY: Cambridge University Press; 1992.
24. Lindeberg T. Feature detection with automatic scale selection. Int J Comput Vision 1998;30:79–116.
25. Chefd'hotel C, Hermosillo G, Faugeras O. Flows of Diffeomorphisms for Multimodal Image Registration. In: 2000 IEEE International Symposium on Biomedical Imaging, July 7–10, 2002, Washington D.C., USA. pp 753–756.
26. Nelder JA, Mead R. A simplex method for function minimization. Comput J 1965;7:308–313.
27. Marquardt DW. An algorithm for least-squares estimation of nonlinear parameters. J Soc Ind Appl Math 1963;11:431–441.
28. Dice LR. Measures of the amount of ecologic association between species. Ecology 1945;26:297–302.
29. Zijdenbos AP, Dawant BM, Margolin RA, Palmer AC. Morphometric analysis of white matter lesions in MR images: method and validation. IEEE Trans Med Imaging 1994;13:716–724.
30. Milles J, van der Geest RJ, Jerosch-Herold M, Reiber J, Lelieveldt B. Fully automated motion correction in first-pass myocardial perfusion MR image sequences. IEEE Trans Med Imaging 2008;27:1611–1621.
31. Ablitt NA, Jianxin G, Keegan J, Stegger L, Firmin DN, Guang-Zhong Y. Predictive cardiac motion modeling and correction with partial least squares regression. IEEE Trans Med Imaging 2004;23: 1315–1324.
32. Ding Y, Chung Y-C, Raman SV, Simonetti OP. Application of the Karhunen–Loeve transform temporal image filter to reduce noise in real-time cardiac cine MRI. Phys Med Biol 2009;54:3909.
33. Kellman P, Chefd'hotel C, Lorenz CH, Mancini C, Arai AE, McVeigh ER. Fully automatic, retrospective enhancement of real-time acquired cardiac cine MR images using image-based navigators and respiratory motion-corrected averaging. Magn Reson Med 2008;59:771–778.